SAND2017-10955J

Lagrangian technique to calculate window interface velocity from shock velocity measurements: application for quartz windows

Chad A. McCoy[1], Marcus D. Knudson[1,2]

[1]*Sandia National Laboratories, Albuquerque, NM 87185, USA*

[2]*Institute for Shock Physics, Washington State University, Pullman, WA 99164, USA*

Measurement of the window interface velocity is a common technique for investigating the dynamic response materials at high strain rates. However, these measurements are limited in pressure to the range where the window remains transparent. The most common window material for this application is lithium fluoride, which under single shock compression becomes opaque at ~200 GPa. To date no other window material has been identified for use at higher pressures. Here we present a Lagrangian technique to calculate the interface velocity from a continuously measured shock velocity, with application to quartz. The quartz shock front becomes reflective upon melt, at ~100 GPa, enabling the use of velocity interferometry to continuously measure the shock velocity. This technique overlaps with the range of pressures accessible with LiF windows and extends the region where wave profile measurements are possible to pressures in excess of 2000 GPa. We show through simulated data that the technique accurately reproduces the interface velocity within 20% of the initial state, and that the Lagrangian technique represents a significant improvement over a simple linear approximation.

Introduction

The development of laser interferometry enabled time-resolved measurement of the velocity of a reflective surface.[1] This allowed for the measurement of free surface and window

interface velocities in dynamic compression experiments. These measurements have yielded valuable data on the compressive behavior and strength of materials during both shock[2-4] and ramp compression[5, 6] and release.[3, 4]

One complication of window interface measurements is the unavoidable presence of wave interactions caused by wave reflections due to impedance mismatch at the interface. Recent efforts have gone towards improvement of the analysis of such experiments to better infer in-material velocity from the window interface velocity. Initial techniques include the self-consistent method[3] and incremental impedance matching method,[4] which correct for the different impedance of the window and sample, but not the variable wave speed in the material due to characteristic interactions. Later techniques, such as the backwards characteristics analysis method[7, 8] (BCAM, also referred to as iterative Lagrangian analysis) and transfer function method[5, 6] (TFM), account for the bending of characteristics due to wave interactions and significantly improve the accuracy of the analysis compared to the earlier techniques.

In common between all the described techniques is a reliance on the free surface or window interface velocity profile. In the case of window interface measurement this limits the range of pressures over which experiments can be performed to that where the window is transparent and the interface velocity can be recorded. Lithium fluoride (LiF) is commonly used as a window material for shock and ramp compression experiments; LiF has been demonstrated to remain transparent to ~200 GPa under single shock compression[9, 10] and ~800 GPa under ramp compression.[11, 12] Under shock compression, most materials melt at low enough temperatures for LiF to be a viable window material. However, high-strength materials, such as diamond[13-17] and beryllium,[18, 19] can have higher melting points, above 200 GPa where LiF is no longer transparent. For such materials, a different window material needs to be identified. To date no

other material has been identified as a suitable window for these types of experiments at shock pressures above 200 GPa.

Many transparent materials, including plastics[20], aerogels[21-23], glasses[24-30], and crystals[13-16, 26-32], have been shown to shock melt into a conductive fluid with reflective shock fronts at pressures as low as 100 GPa. If the interface velocity could be calculated from the measured shock velocity, any of these materials could serve as a viable window for wave profile measurements in the multi-Mbar regime, provided that the equation of state (EOS) of the material is well known. This technique can be used for pressures in excess of 2000 GPa[33, 34], significantly greater than the shock-melting pressure of any previously studied material.

Here we describe a Lagrangian technique to calculate the sample-window interface velocity from the measured shock velocity in the window and discuss the application of this technique to quartz windows, which have well-characterized shock and release responses. This is similar to the technique described by Nikolaev *et al* using a linear characteristic model to relate the radiation history of a shock front in bromoform to the particle velocity at a bromoform-sapphire interface.[35, 36] The Lagrangian technique uses knowledge of the sound velocity at the pressure-density conditions accessed in shock-release experiments. Using simulated data, we demonstrate that the Lagrangian technique accurately reproduces the interface particle velocity along the release for velocities within 20% of the initial particle velocity. The technique is also shown to be a significant improvement over a linear characteristic model, particularly in cases where time dependent phenomena may be encountered.

Characteristics method

Similar to the BCAM and TFM techniques, our analysis code is developed to determine the in-material properties from observation of velocity at an interface. However, in this

technique the interface is not a fixed surface between a sample and window, but a moving boundary between shocked and unshocked material in the window. Hence, in the Lagrangian $x-t$ frame, the characteristics are no longer bounded by fixed coordinates, but by a fixed coordinate at the sample-window interface and a moving coordinate at the shock front as seen in Figure 1. The Lagrangian coordinate at the shock front, $D(t_S)$, is defined as

$$D(t_S) = \int_0^{t_S} U_S(t')dt', \tag{1}$$

where $U_S(t')$ is the measured shock velocity at time t'.

We use the conventional definition of the Riemann invariants with respect to density along the characteristics[37, 38], such that

$$R^{\pm} = u_p \pm \int_{\rho_0}^{\rho_H} \frac{C_S(\rho)}{\rho} d\rho, \tag{2}$$

where u_p is the particle velocity, $C_S(\rho)$ is the isentropic sound velocity, ρ is the density along the isentrope, and ρ_0 and ρ_H are the initial density and shocked density of the window. The properties at the shock front are determined from the Rankine-Hugoniot relations, which give

$$\frac{\rho}{\rho_0} = \frac{U_S}{U_S - u_p}, \text{ and} \tag{3}$$

$$P = \rho_0 U_S u_p \tag{4}$$

where P is the pressure. Because the integral in the Riemann invariant in Eq. 2 is defined along an isentrope, the isentrope that intersects the shock state is calculated and the sound velocity is given as $C_S^2 = \left.\frac{dP}{d\rho}\right|_S$ for every Lagrangian coordinate, $D(t_S)$. The Riemann invariant is calculated at the shock front for both the positive (C^+) and negative (C^-) characteristics under the assumption that the isentrope at the shocked state is known. For the shock to be reflective,

the window must have melted into a conductive fluid, hence it can be assumed that the release is isentropic. In this case, the release can be determined either from a tabular EOS model, such as SESAME, or from an analytic model such as a Mie-Grüneisen EOS.

Within the window, the C^+ and C^- characteristics are propagated backwards from the shock front at the Lagrangian sound velocity, $C_L = \frac{\rho}{\rho_0} C_S$, which defines the local slope in the $x-t$ frame. At intersections between positive and negative characteristics, the particle velocity is given as

$$u_p = \frac{R^+ + R^-}{2}. \tag{5}$$

We assume that the $P-\rho$ state of a particular Lagrangian coordinate lies on the release intersecting its Hugoniot state. Calculating the release of the Hugoniot state at the Lagrangian coordinate where intersection occurs determines the isentropic sound velocity as a function of the particle velocity along the release. The sound velocity is then determined by interpolating along the release for the particle velocity determined from Eq. 5. The sound velocity between intersections is assumed to be constant and equal to the sound velocity determined at the previous intersection along the particular characteristic.

This procedure is repeated for all intersections between positive and negative characteristics between the shock front and the sample-window interface. Because the sound velocity along a given C^- characteristic depends on the intersections with positive characteristics, the intersections must be mapped simultaneously forward in time and backward in space. This is done by following C^+ initiating at later times along the shock front back to the interface. The initial C^+ characteristic reaches the shock front at the moment the rarefaction overtakes the shock. Therefore, at a given Lagrangian position, prior to arrival of the first C^-

characteristic, the positive characteristics are all simple waves. At later times, the positive characteristics interact with negative characteristics, changing the local sound velocity and the slope of the characteristics. In particular, the C_j^+ characteristic will intersect all C_i^- characteristics, provided that $i < j$ and the C_i^- characteristics have not reached the sample-window interface prior to the C_j^+ characteristic entering the window. We chose to ignore reflections of the characteristics at the sample-window interface and second-order intersections in this analysis.

The particle velocity at the sample-window interface along a given C^+ is defined as the particle velocity from Eq. 5 of the characteristic intersection closest to the interface. Similarly, the time at the interface is found from interpolating the C^+ characteristic for zero Lagrangian depth. These values build the interface profile shown in Figure 2.

Simulation of shock experiments

To evaluate the accuracy of the Lagrangian technique we appealed to simulated data using the 1-D Lagrangian magnetohydrodynamics code LASLO[39], a lightweight analogue of the more mature ALEGRA code[40]. In the simulations, a tracer was positioned at the interface between the sample (either copper or diamond) and the quartz window. Additional tracers were uniformly spaced every 2 μm through the quartz window. The shock position as a function of time was determined by identifying the times at which the particle velocity along the subsequent tracers reached 10% of the maximum value for a given position. The derivative of the shock position as a function of time provides the shock velocity, which was used in the Lagrangian technique described in the previous section. Characteristics were initiated from each Lagrangian coordinate along the shock front. The resulting inferred particle velocity at the sample-window interface obtained from the Lagrangian technique was then compared directly to the simulated

particle velocity at the corresponding tracer location. The results were also compared to the linear characteristic model which assumes the sound velocity, C_L, along each characteristic is constant, such that the time at the interface, t_I, is simply $t_I = t_S - \frac{D(t_S)}{C_L}$. In this approximation the particle velocity at the interface is set equal to that at the shock front along the given characteristic.

The EOS models used in the simulations were SESAME 3700 (aluminum), SESAME 3325 (copper), LEOS 7899 (diamond, a 5-phase Purgatorio-based table that includes phase transitions and melting along the principal Hugoniot), and SESAME 90010 (quartz). In order to simplify calculations using the Lagrangian technique a Mie-Grüneisen, linear reference (MGLR) constant Gamma model, similar to the experimental quartz MGLR model developed by Knudson and Desjarlais, was constructed for the SESAME 90010 table. This was accomplished by optimizing the effective Gamma, Γ_{eff}, over numerous SESAME 90010 release paths for quartz shock velocities ranging from ~11-25 km/s (160-1050 GPa). A comparison between Γ_{eff} calculated from the experimental results (black line) and the SESAME 90010 table (red diamonds and dashed line) is shown in Figure 3a. This enabled a completely analytical calculation for the Lagrangian technique.

The release curves calculated using the MGLR model with Γ_{eff} from SESAME (dashed lines) have slightly less curvature than those calculated directly from SESAME (solid lines) as seen in Figure 3b. This results in the local sound velocity being underpredicted at high pressures and overpredicted at lower pressures along a given release path, which impacts the calculated Riemann invariants and intersection particle velocities. In particular, the C^- characteristic used in determining the particle velocity at the interface would be shifted to a higher pressure initial

state and be artificially high due to a decrease in the value of the integral in Eq. 2. This produces interface velocities that are inflated over the range of pressures where the MGLR release curve lies above the SESAME result.

The first case considered was a simple shock and release simulation where the sample fully melts and no strength remains in the sample. The simulation consisted of an aluminum-backed copper flyer plate impacting a copper baseplate backed with a quartz window at 20 km/s. At this impact velocity the shock is sufficiently strong to fully melt the copper, thus the rarefaction from the Cu/Al interface in the flyer produces a simple, featureless release as seen in Figure 4. For this simple case, both the Lagrangian technique (black dashed line) and the linear approximation (blue dotted line) reasonably reproduce the simulated interface particle velocity (red line). In particular, the arrival time of the release overtake at the window-sample interface is accurately determined with both techniques. However, the initial rate of release is over-predicted by the linear approximation, while it is well described by the Lagrangian technique. Further down the release, the agreement with the interface velocity lessens for both the linear approximation and Lagrangian technique. This is particularly true with respect to the velocity plateau; both methods differ by ~2% from the simulated results. In this simulation, the initial shock in the quartz was ~800 GPa and decayed to ~450 GPa at the velocity plateau. From Figure 3b, the MGLR release lies above the SESAME release over range of pressures in this simulation, generating the inflated particle velocity seen in the Lagrangian technique as discussed earlier. We note, however, that the time at which the interface reaches the velocity plateau is better reproduced by the Lagrangian technique.

The second case considered was a shock and release simulation in a solid, assuming an ideal elastic-plastic response. With the addition of strength, the system becomes more

complicated due to interactions between elastic and plastic waves in the sample. To model this case, an identical flyer to the previous example was impacted into a diamond sample backed by a quartz window at an impact velocity of 14 km/s. This impact generates a ~600 GPa shock in the diamond. The diamond was modeled as a rate-independent purely elastic-plastic solid, and the material was assumed to be overdriven at 600 GPa, so there was no elastic precursor at the diamond/quartz interface. The inferred particle velocity at the sample-window interface for the linear approximation and the Lagrangian technique are compared to the simulated result in Figure 5. For particle velocities above 8 km/s, the Lagrangian technique reasonably reproduces the simulated profile due to the small change in pressure from the initial shock state. In contrast the linear approximation slightly underpredicts the velocity at the second plateau, prior to overtake of the bulk release. Similar to the previous case, the difference between SESAME and MGLR releases produces a particle velocity ~2% high at the final velocity plateau, but accurately reproduces the time at which the plateau occurs for the Lagrangian case. The divergence of the linear approximation is more pronounced in this example as it initially underpredicts the interface velocity, but at later time predicts a higher velocity than both the simulation and Lagrangian technique. The interface is also predicted to reach the final velocity plateau ~3 ns later for the linear approximation than the simulation or Lagrangian analysis.

The final case considered included a rate-dependent Steinberg-Guinan-Lund (SGL)[41] strength model which includes work hardening, strain hardening, and thermal softening. Because the Lagrangian technique assumes the behavior in the quartz window is rate-independent, this simulation provides a strenuous test of the accuracy of the technique due to the complicated behavior of diamond. As in the previous case, the diamond strength was adjusted such that the shock in the simulation was overdriven so as to transmit a single shock into the

quartz window, rather than a two-wave structure with an elastic precursor. This was necessary to accurately calculate the displacement of the shock in the quartz window from the simulated shock velocity.

The SGL model also allows for modification of the $P-T$ dependence of the melt curve such that shock melting occurs at different pressures along the Hugoniot. In this simulation, the melt temperature along the Hugoniot was set at 7000 K, just below the temperature reached in the peak shocked state of the simulation. The negative Clapeyron slope in the SESAME model for diamond, consistent with experimental measurements of Brygoo *et al*[16] and Eggert *et al*,[15] resulted in the diamond sample undergoing a liquid-solid phase transition upon release. This transition is manifest in the simulation by a rarefaction shock in the diamond. As shown in Figure 6, both the linear approximation and Lagrangian technique reasonably reproduce the initial release in the liquid diamond. This is expected because above the shock-melt transition, the diamond has no strength and the release is therefore rate-independent. However, across the transition, the behavior becomes rate-dependent due to the onset of strength. At the liquid-solid transition, a rarefaction shock occurs in the simulation. The Lagrangian technique successfully captures both the magnitude and arrival time of the rarefaction shock at the sample-window interface, as well as the initial slope of the release in the solid diamond. Similar to the previous examples, the Lagrangian technique overpredicts the particle velocity for velocities below ~80% of the initial steady state velocity. Unlike the previous examples, the linear approximation does a very poor job of representing the particle velocity at the interface. In particular, the linear approximation does not reproduce the rarefaction shock at the liquid-solid transition and the velocity is significantly different for all later times.

Application to quartz windows:

α-Quartz is an ideal material for high-pressure windows due to its well-defined Hugoniot and release behavior, with both experimentally constrained in excess of 1200 GPa[33, 42] and further constrained by first-principles molecular dynamics calculations to 3000 GPa.[43] Shocks in quartz have been demonstrated to be reflective for pressures around 100 GPa[28], which enables overlap with transparent LiF windows due to their closely-matched impedances. Fratanduono *et al*[44] and McCoy *et al*[45] have demonstrated that the sound velocity calculated from the quartz release model developed by Knudson and Desjarlais[42] accurately reproduces the quartz sound velocity over the entire high-pressure liquid regime. This satisfies the criterion for the Lagrangian technique of knowledge of the EOS and sound velocity at all states intersected by a shock and release experiment.

As an example, we show in Figure 7 results from recent experiments investigating the sound velocity in beryllium which used both quartz and LiF windows for wave profile measurements. These experiments impacted copper-faced aluminum flyers into stepped beryllium targets (steps ranging from 500-1100 μm) at velocities ranging from 7-13 km/s. A full description of the experiments and results will be the subject of a future publication. For the quartz (Figure 7a), the shock velocity (thin blue lines) was measured for each step and the Lagrangian technique was used to determine the interface profiles (thick black lines) using the experimentally determined Hugoniot and MGLR release model for quartz (black solid line in Fig. 3). In the LiF (Figure 7b), the interface profile (green dashed-dotted lines) is measured directly for each step and the profiles are compared to the time-shifted quartz profiles. The interface profiles in both cases are similar with both exhibiting a 2-wave (longitudinal and bulk) release structure in the beryllium.

Conclusions:

We developed a Lagrangian technique to use the shock velocity in a transparent window to infer sample-window interface wave profiles at pressures in excess of traditional interface measurement techniques. The technique uses knowledge of the sound velocity to account for nonlinear characteristics while propagating the shock velocity profile back to the sample-window interface. Analysis of simulated experiments demonstrates that the Lagrangian technique adequately accounts for bending of characteristics and better reproduces the interface particle velocity than the linear characteristic approximation. The simulations show that for particle velocities within 20% of the initial velocity, the Lagrangian technique reasonably reproduces the interface velocity in both rate-independent and rate-dependent cases. We also utilize the Hugoniot and release model of α-quartz to produce sample-window interface profiles from recent experimental measurements of Be in the multi-Mbar regime and show that α-quartz is an ideal material to supplement LiF windows at high pressure.

Acknowledgements:

We would like to thank Jean-Paul Davis and Steve Rothman for their discussions on characteristic analysis and calculating the sound velocity from the Riemann invariants. We also thank Justin Brown for his explanation of the strength models in LASLO. Sandia National Laboratories is a multimission laboratory managed and operated by National Technology and Engineering Solutions of Sandia, LLC, a wholly owned subsidiary of Honeywell International, Inc., for the U.S. Department of Energy's National Nuclear Security Administration under contract DE-NA0003525.

References:

1. L. M. Barker and R. E. Hollenbach, J. Appl. Phys. **43** (11), 4669–4675 (1972).
2. T. J. Ahrens, W. Gust and E. Royce, J. Appl. Phys. **39** (10), 4610-4616 (1968).

3. J. Asay and J. Lipkin, J. Appl. Phys. **49** (7), 4242-4247 (1978).

4. J. Lipkin and J. Asay, J. Appl. Phys. **48** (1), 182-189 (1977).

5. J. Brown, C. Alexander, J. Asay, T. Vogler and J. Ding, J. Appl. Phys. **114** (22), 223518 (2013).

6. J. Brown, C. Alexander, J. Asay, T. Vogler, D. Dolan and J. Belof, J. Appl. Phys. **115** (4), 043530 (2014).

7. J. R. Maw, AIP Conf. Proc. **706** (1), 1217-1220 (2004).

8. S. Rothman, J. Davis, J. Maw, C. Robinson, K. Parker and J. Palmer, J. Phys. D: Appl. Phys. **38** (5), 733 (2005).

9. M. Furnish, L. Chhabildas and W. Reinhart, Int. J. Imp. Engin. **23** (1), 261-270 (1999).

10. P. Rigg, M. Knudson, R. Scharff and R. Hixson, J. Appl. Phys. **116** (3), 033515 (2014).

11. D. E. Fratanduono, T. R. Boehly, M. A. Barrios, D. D. Meyerhofer, J. H. Eggert, R. F. Smith, D. G. Hicks, P. M. Celliers, D. G. Braun and G. W. Collins, J. Appl. Phys. **109** (12), 123521 (2011).

12. J.-P. Davis, M. D. Knudson, L. Shulenburger and S. D. Crockett, J. Appl. Phys. **120** (16), 165901 (2016).

13. D. Bradley, J. Eggert, D. Hicks, P. Celliers, S. Moon, R. Cauble and G. Collins, Phys. Rev. Lett. **93** (19), 195506 (2004).

14. M. D. Knudson, M. P. Desjarlais and D. H. Dolan, Science **322** (5909), 1822–1825 (2008).

15. J. Eggert, D. Hicks, P. Celliers, D. Bradley, R. McWilliams, R. Jeanloz, J. Miller, T. Boehly and G. Collins, Nature Physics **6** (1), 40-43 (2010).

16. S. Brygoo, E. Henry, P. Loubeyre, J. Eggert, M. Koenig, B. Loupias, A. Benuzzi-Mounaix and M. R. Le Gloahec, Nature materials **6** (4), 274-277 (2007).

17. K. V. Khishchenko, V. E. Fortov, I. V. Lomonosov, M. N. Pavlovskii, G. V. Simakov and M. V. Zhernokletov, AIP Conf. Proc. **620** (1), 759-762 (2002).

18. M. D. Knudson, AIP Conf. Proc. **1426**, 35-42 (2012).

19. L. X. Benedict, T. Ogitsu, A. Trave, C. J. Wu, P. A. Sterne and E. Schwegler, Phys. Rev. B **79**, 064106 (2009).

20. M. A. Barrios, D. G. Hicks, T. R. Boehly, D. E. Fratanduono, J. H. Eggert, P. M. Celliers, G. W. Collins and D. D. Meyerhofer, Phys. Plasmas **17** (5), 056307 (2010).

21. J. E. Miller, T. R. Boehly, D. D. Meyerhofer and J. H. Eggert, Shock Compression of Condensed Matter–2007 **955**, 71–74 (2007).

22. K. Falk, C. A. McCoy, C. L. Fryer, C. W. Greeff, A. L. Hungerford, D. S. Montgomery, D. W. Schmidt, D. G. Sheppard, J. R. Williams, T. R. Boehly and J. F. Benage, Phys. Rev. E **90** (3), 033107 (2014).

23. M. D. Knudson and R. W. Lemke, J. Appl. Phys. **114** (5), 053510 (2013).

24. C. A. McCoy, M. C. Gregor, D. N. Polsin, D. E. Fratanduono, P. M. Celliers, T. R. Boehly and D. D. Meyerhofer, J. Appl. Phys. **119** (21), 215901 (2016).

25. Y. B. Zel’dovich, S. B. Kormer, M. B. Sinitsyn and A. I. Kuryapin, Dokl. Akad. Nauk. **122**, 48-50 (1958).

26. Y. B. Zel'Dovich, S. B. Kormer, M. V. Sinitsyn and K. B. Yushko, Dokl. Akad. Nauk **138**, 1333 (1961).

27. S. B. Kormer, Physics-Uspekhi **11** (2), 229-254 (1968).

28. J. A. Akins and T. J. Ahrens, Geophysical Research Letters **29** (10), 31-31-31-34 (2002).

29. D. G. Hicks, T. R. Boehly, J. H. Eggert, J. E. Miller, P. M. Celliers and G. W. Collins, Phys. Rev. Lett. **97** (2), 025502 (2006).

30. D. Spaulding, R. McWilliams, R. Jeanloz, J. Eggert, P. Celliers, D. Hicks, G. Collins and R. Smith, Phys. Rev. Lett. **108** (6), 065701 (2012).

31. R. S. McWilliams, D. K. Spaulding, J. H. Eggert, P. M. Celliers, D. G. Hicks, R. F. Smith, G. W. Collins and R. Jeanloz, Science **338** (6112), 1330-1333 (2012).

32. D. G. Hicks, P. M. Celliers, G. W. Collins, J. H. Eggert and S. J. Moon, Phys. Rev. Lett. **91** (3), 035502 (2003).

33. M. D. Knudson and M. P. Desjarlais, Phys. Rev. Lett. **103** (22), 225501 (2009).

34. R. F. Trunin, Physics-Uspekhi **44** (4), 371-396 (2001).

35. D. N. Nikolaev, A. S. Filimonov, V. E. Fortov, I. V. Lomonosov and V. Y. Ternovoi, AIP Conf. Proc. **429** (1), 509-512 (1998).

36. D. N. Nikolaev, A. A. Pyalling, K. V. Khishchenko, V. Y. Ternovoi and V. E. Fortov, Chem. Phys. Rep. **19** (10), 1967-1990 (2001).

37. R. Courant and K. O. Friedrichs, *Supersonic Flow and Shock Waves*. (Springer-Verlag, New York, 1976).

38. Y. B. Zel'dovich and Y. P. Raizer, *Physics of Shock Waves and High-Temperature Hydrodynamic Phenomena*. (Dover Publications, 2002).

39. J. H. Carpenter, *private communication* (2016).

40. A. Robinson, T. Brunner, S. Carroll, R. Drake, C. Garasi, T. Gardiner, T. Haill, H. Hanshaw, D. Hensinger and D. Labreche, presented at the 46th AIAA Aerospace Sciences Meeting and Exhibit, 2008 (unpublished).

41. D. Steinberg and C. Lund, J. Appl. Phys. **65** (4), 1528-1533 (1989).

42. M. D. Knudson and M. P. Desjarlais, Phys. Rev. B **88** (18), 184107 (2013).

43. M. P. Desjarlais, M. D. Knudson and K. R. Cochrane, J. Appl. Phy. **122** (3), 035903 (2017).

44. D. Fratanduono, P. Celliers, D. Braun, P. Sterne, S. Hamel, A. Shamp, E. Zurek, K. Wu, A. Lazicki and M. Millot, Phys. Rev. B **94** (18), 184107 (2016).

45. C. A. McCoy, M. C. Gregor, D. N. Polsin, D. E. Fratanduono, P. M. Celliers, T. R. Boehly and D. D. Meyerhofer, J. Appl. Phys. **120** (23), 235901 (2016).

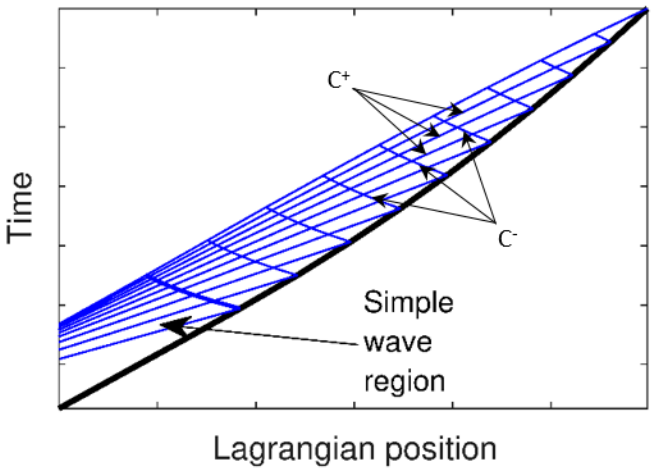

Figure 1: In the Lagrangian frame, the interface remains fixed and the shock front (black) propagates to the right. When shock pressure is constant, characteristics (blue) propagate in a simple wave region without interaction. After reflection of the first characteristic, subsequent C^+ characteristics interact with the reflected C^- characteristics and bend due to changing sound velocity. The analysis technique starts with first characteristic and propagates simultaneously later in time and towards the interface.

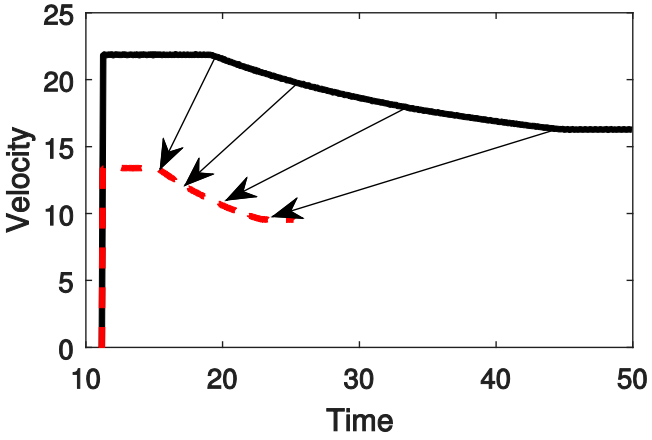

Figure 2: Propagation of characteristics back to sample-window interface determines the time at which the rarefaction reached the interface and assigns a particle velocity through characteristic interaction.

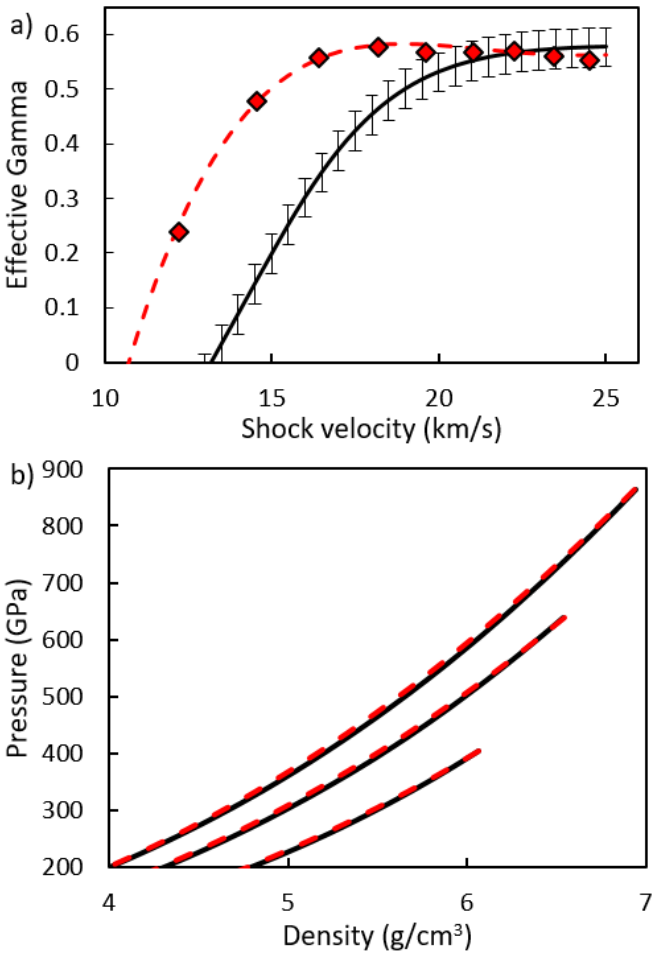

Figure 3: (a) The effective Grüneisen parameter calculated using multiple release curves from the SESAME 90010 model (red diamonds) and a fit to those results (red dashed line) agree with the experimentally derived model (black line) for shock velocities greater than 20 km/s in quartz. Below 20 km/s, the value from SESAME remains approximately constant to ~15 km/s where it drops rapidly. The experimental model begins decreasing for velocities below 20 km/s, but with a slightly lower slope than the SESAME table. (b) The release curves calculated with the MGLR fit to SESAME (dashed lines) display less curvature than those calculated directly from SESAME 90010 (black lines). The shallower curvature decreases the sound velocity along the release curves and can impact the calculated particle velocity at the interface.

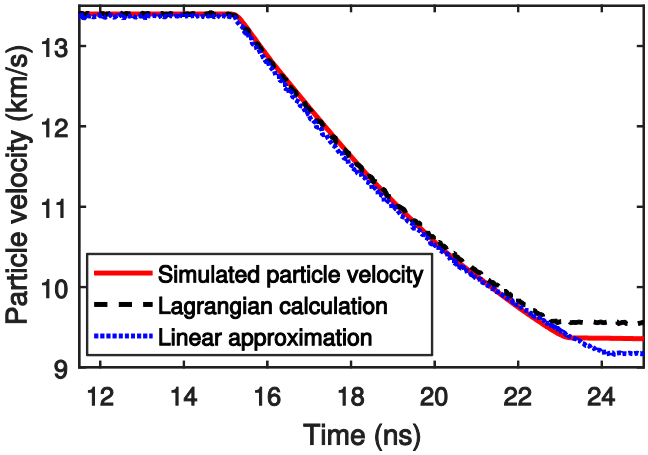

Figure 4: In the simple release case, both the Lagrangian technique (black dash) and linear approximation (blue dot) accurately reproduce the simulated result (red solid). The steady state time at the tail of the release is better inferred by the Lagrangian technique.

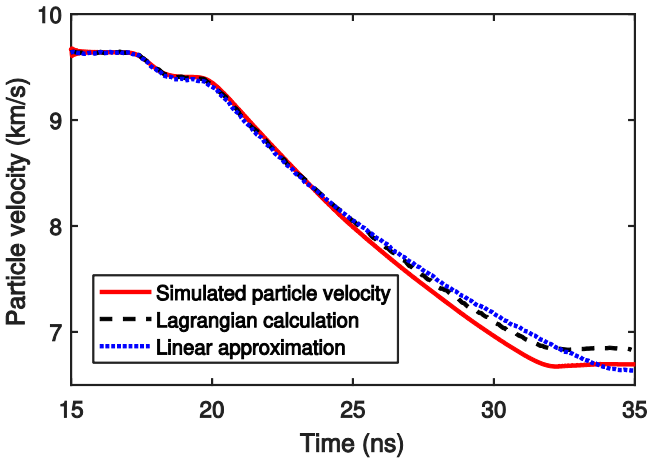

Figure 5: (Lines same as Figure 4) Assuming an elastic-plastic response, the Lagrangian technique matches the simulation for velocities above ~8 km/s. The linear approximation slightly underpredicts the particle velocity at the plateau prior to bulk release and reaches the final plateau at a noticeably later time.

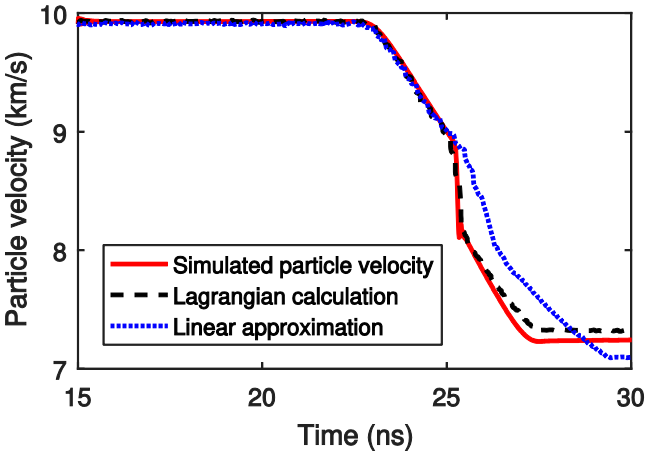

Figure 6: (Lines same as Figure 4) The simulation incorporating the SGL model with an artificially lowered melting point has the most significant difference between the Lagrangian technique and linear approximation. The solidification upon release results in a rarefaction shock in the simulation, which is reproduced in the Lagrangian calculation. The linear approximation fails to reproduce this feature or the behavior at later times.

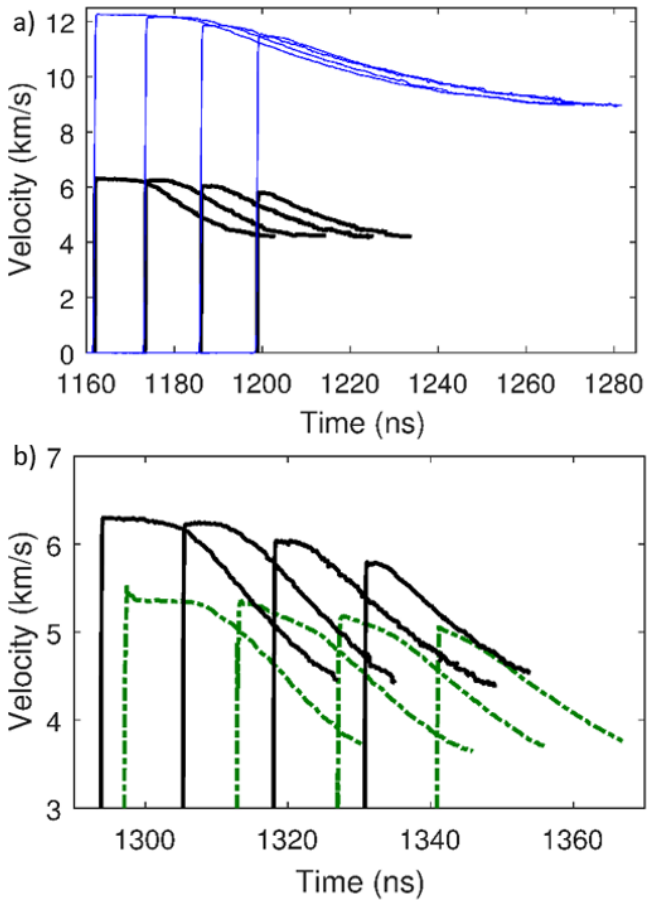

Figure 7: (a) The measured shock velocity profiles in a quartz window (thin blue lines) are used with the Lagrangian technique to determine the sample-window interface profiles (thick black lines). (b) The wave profiles inferred using the quartz window (black solid lines) exhibit a similar shape to those directly obtained using LiF windows at slightly lower pressure (green dashed-dotted lines), with both sets of profiles exhibiting a longitudinal and bulk release in the beryllium. The quartz profiles in (b) are the same as those in (a) with the time axis adjusted to overlap the LiF profiles.